water

MDPI

Article

A Case Study for Analysis of Stability and Treatment Measures of a Landslide Under Rainfall with the Changes in Pore Water Pressure

Liangzhi Tang [1,2], Yun Yan [1,2,*], Faming Zhang [3], Xiaokai Li [3], Yuhong Liang [1,2], Yuru Yan [1,2], Huaqing Zhang [3] and Xiaolong Zhang [3]

[1] Marine Geological Survey of Jiangsu Province, Nanjing 210007, China; liangzhi@126.com (L.T.); yuruyan160@yeah.net (Y.Y.); liangyuhongwu@163.com (Y.L.)
[2] Key Laboratory of Coastal Salt Marsh Ecosystems and Resources, Ministry of Natural Resources, Nanjing 210007, China
[3] School of Earth Sciences and Engineering, Hohai University, Nanjing 211100, China; zhangfm@hhu.edu.cn (F.Z.); 221309080014@hhu.edu.cn (X.L.); 231309080030@hhu.edu.cn (H.Z.); 231309080031@hhu.edu.cn (X.Z.)
* Correspondence: yanyun1606565@126.com; Tel.: +86-187-5185-5163

Abstract: Mining causes damage to the soil and rock mass, while rainfall has a pivotal impact on the mining slope stability, even leading to geological hazards such as landslides. Therefore, the study evaluated the mine landslide stability and determined the effectiveness of the treatment measures under the impact of pore water pressure changes caused by rainfall, taking the Kong Mountain landslide in Nanjing, Jiangsu Province, China, as the research object. The geological conditions and deformation characteristics were clarified, and the failure mechanism and influencing factors were analyzed. Also, the landslide stability was comprehensively evaluated and calculated utilizing the finite element-improved limit equilibrium method and FLAC 3D 6.0, which simulated the distribution of pore water pressure, displacement, etc., to analyze the influence of rainfall conditions and reinforcement effects. The results indicated the following: (1) Rainfall is the key influencing factor of the landslide stability, which caused the pore water pressure changes and the loosening of the soil due to the strong permeability; (2) The distribution of the pore water pressure and plastic zone showed that, during the rainfall process, a large area of transient saturation zone appeared at the leading edge, affecting the stability of the whole landslide and led to the further deformation; (3) After the application of treatment measures (anti-sliding piles and anchor cables), the landslide stability increased under both natural and rainfall conditions (from 1.02 and 0.94 to 1.38 and 1.31, respectively), along with a reduction in displacement, plastic zones, etc. The Kong Mountain landslide, with the implemented treatment measures, is in good stability, which is in line with the evaluation and calculation results. The study provides certain contributions to the stability evaluation and treatment selection of similar engineering under rainfall infiltration.

Keywords: rainfall-induced landslide; stability analysis; treatment measures; pore water pressure; numerical simulation

check for updates

Citation: Tang, L.; Yan, Y.; Zhang, F.; Li, X.; Liang, Y.; Yan, Y.; Zhang, H.; Zhang, X. A Case Study for Analysis of Stability and Treatment Measures of a Landslide Under Rainfall with the Changes in Pore Water Pressure. *Water* **2024**, *16*, 3113. https://doi.org/10.3390/w16213113

Academic Editor: Gang Mei

Received: 19 September 2024
Revised: 25 October 2024
Accepted: 26 October 2024
Published: 30 October 2024

Copyright: © 2024 by the authors. Licensee MDPI, Basel, Switzerland. This article is an open access article distributed under the terms and conditions of the Creative Commons Attribution (CC BY) license (https://creativecommons.org/licenses/by/4.0/).

1. Introduction

Mining causes damage to the soil and rock mass on the mining slopes, severely disturbing the geological environment, This disturbance causes a significant threat to the safety of mining slopes and can even lead to geological hazards such as landslides. The mining slope stability is affected by various unfavorable factors, especially rainfall [1–4], which can cause continuous compression deformation or local deformation of the landslide body, thereby increasing the likelihood of landslide failure. Therefore, evaluating the stability of mine slopes or potential landslides and exploring the effectiveness of treatment

measures can effectively enhance the safety of mine slopes and achieve the goal of disaster prevention, particularly under the influence of rainfall infiltration.

Nowadays, scholars have conducted various studies on the stability and the mechanism of triggering, deformation, and failure of the mining slopes or landslides. The limit equilibrium method (LEM) is one of the most commonly used methods for analyzing the stability and failure mode of mine slopes under different factors [5–10]. Meanwhile, combined with the LEM, some studies evaluate and predict slope stability with artificial neural networks-optimization algorithms [11] and UAV technology [12]. The influencing factors triggering landslide occurrence are demonstrated by some scholars. Di et al. [13] studied the failure mechanism of sandy slopes with different inclinations under rainfall and proposed a simplified expression according to the soil mechanics theory, considering factors such as soil type, pore water pressure, and the conservation of mass for water and soil [14], etc. Take et al. [15] analyzed the triggering mechanism of fast landslides in fill slopes with the impact of static liquefaction and pore water pressure under rainfall, considering the bedrock depth. Additionally, some theoretical derivations and analyses are conducted to illustrate the deformation and the failure mechanism of mine slopes under rainfall using an equivalent continuum model and dual-continuum model [16], the regional sliding mechanical model [17], the mechanical truncation method [18], etc.

Due to the advantages of the physical model tests in reproducing the deformation and failure process of unstable slopes under rainfall, model tests are conducted to analyze the failure mechanism [19,20], evolution characteristics [21,22], changes of slope stability coefficient [23], etc. Also, numerical analysis methods such as finite element method (FEM) [24,25], finite difference method (FDM) [26,27], and discrete element method (DEM) [28–30] are widely used in the simulation and evaluation of mine slopes and landslides. Although the methods are commonly used for the simulation, there are obstacles to creating realistic simulation results. Therefore, hybrid numerical methods are taken to tackle such obstacles. Sun et al. [31,32] developed the Y-slope approach based on the FDEM to evaluate the rock slope stability and simulate the failure process, combining the continue and discontinue methods. Zhao et al. [33] further improved the FDEM method to simulate the whole motion trajectory of the landslide to evaluate the rock slope stability. Some scholars analyze the instability process and failure mechanism of mining slopes combining the model tests with numerical analysis considering the advantages [34,35].

Based on the literature review, it can be concluded that stability evaluation of some mining landslides involves numerical simulation with simplified 2D or 3D models, often without considering the changes in pore water pressure under different rainfall conditions. Considering the impact of rainfall infiltration on the changes in pore water pressure, based on the field investigation results and indoor rock and soil parameter analysis, pore water pressure distribution under different conditions of the Kong Mountain landslide was simulated with the 2D model (FEM and FEM–LEM), while the effectiveness of the treatment measures was verified with 3D simulation (FLAC 3D 6.0), comparing the displacement, the maximum shear strain and the plastic zone of the landslide with or without the reinforcement. This study is of great practical significance for the stability evaluation of rainfall-induced mining landslides and provides a new perspective for the stability evaluation and treatment measures selection of similar mining landslides.

2. Overview of the Study Area

2.1. Location of the Study Area

The study area is located in the Kong Mountain open-pit mine in Jiangning District, Nanjing City, Jiangsu Province. The study area belongs to the low mountain and hilly landform unit, and the terrain is low in the north and high in the south (Figure 1). After years of mining, the Kong Mountain Mine has formed an exposed slope with a length of about 1.1 km and a maximum height of about 130 m, which is divided into nine slope surfaces and eight steps in the slope.

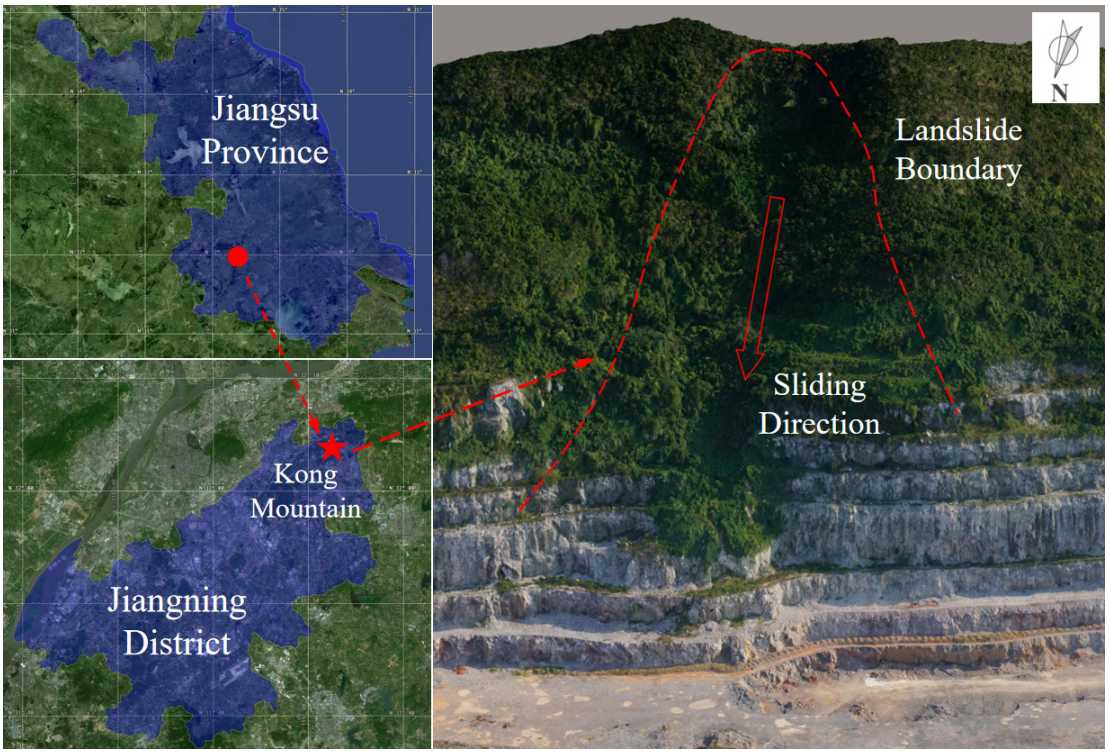


Figure 1. Location and image of the Kong Mountain landslide.

The study area belongs to the northern subtropical monsoon climate, with a humid climate and four distinct seasons. The average annual rainfall in the study area is about 1012.1 mm, with rainfall occurring from April to May, late June to early July, and during the typhoon season in September. Therefore, according to the rainfall characteristics in the study area (Figure 2), the rainfall concentrated in the summer in the study area will affect the landslide deformation, especially the long-term and heavy rainfall under extreme weather.

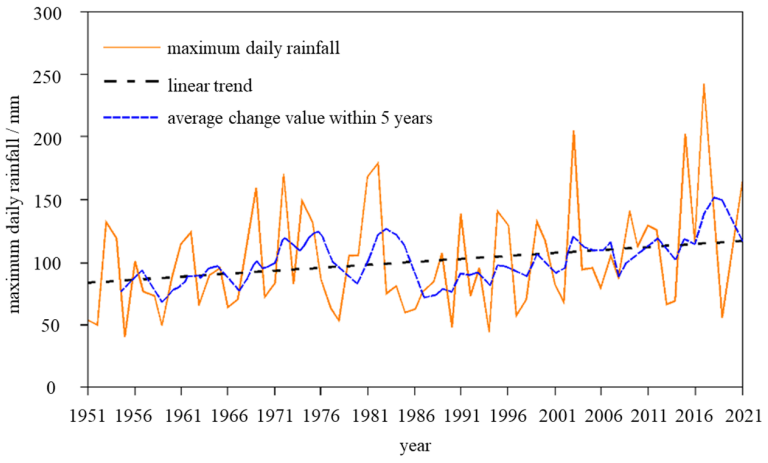


Figure 2. Rainfall characteristics of the study area.

2.2. Engineering Geological Characteristics of the Study Area

According to the field investigation and the information revealed by the drilling core (Figure 3), it can be concluded that the cover layer in the mine slope is mainly composed of residual soil (powdery clay with crushed stones). The lithology and strata of the bedrock include limestone (C_2P_{1c}, C_{2h}), mudstone (C_1), and sandstone (D_{3w}). The borings provide the reference for the cross and longitudinal sections of the landslide (Figure 4). Each rock layer is monoclinic, with an attitude of 196°∠85°. The groundwater mainly consists of

loose pore water and bedrock fissure water with weak connectivity, while the surface water is underdeveloped. Loose pore water exists in the cover layer while the bedrock fissure water is distributed in cracks, joints, and the bedrock.

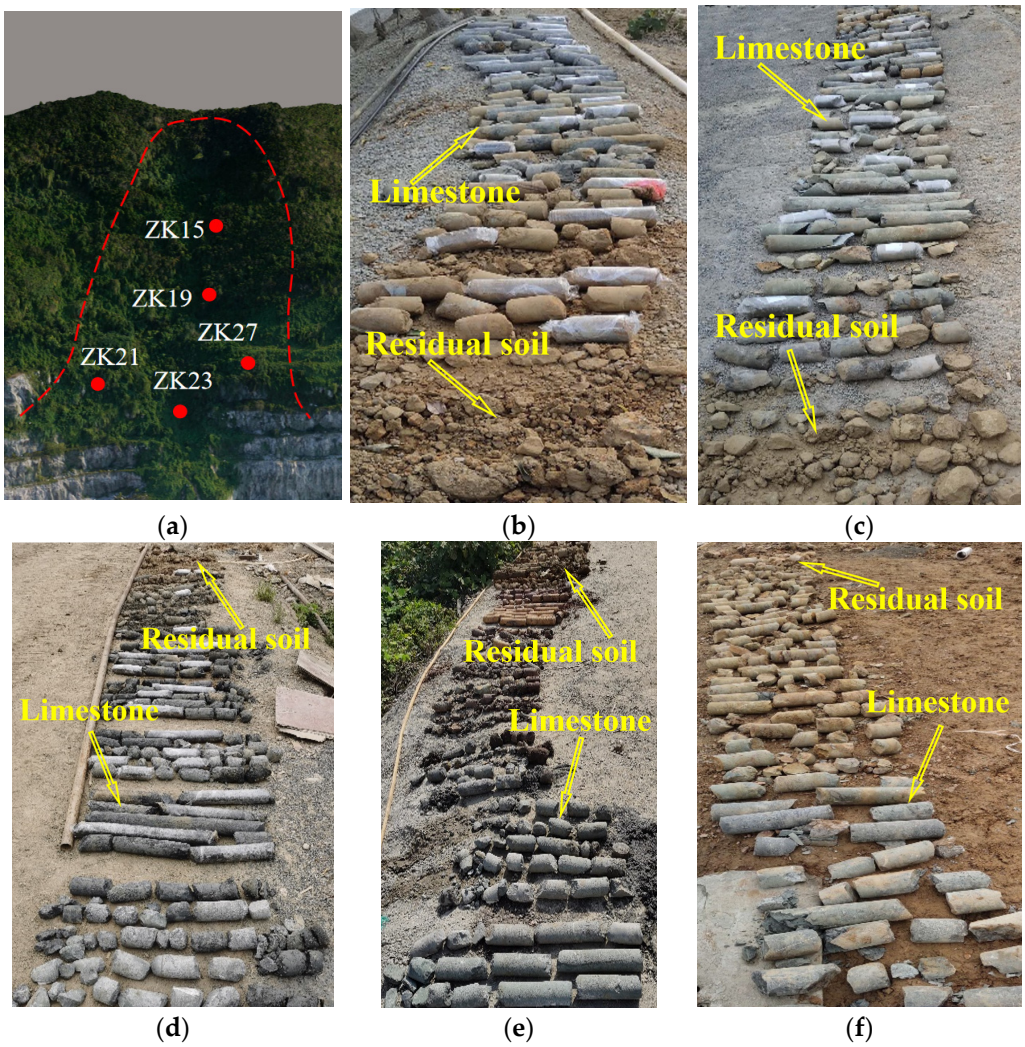


Figure 3. Diagram of the borehole core. (**a**) Boring position; (**b**) ZK15 borehole core; (**c**) ZK19 borehole core; (**d**) ZK23 borehole core; (**e**) ZK27 borehole core; and (**f**) ZK21 borehole core.

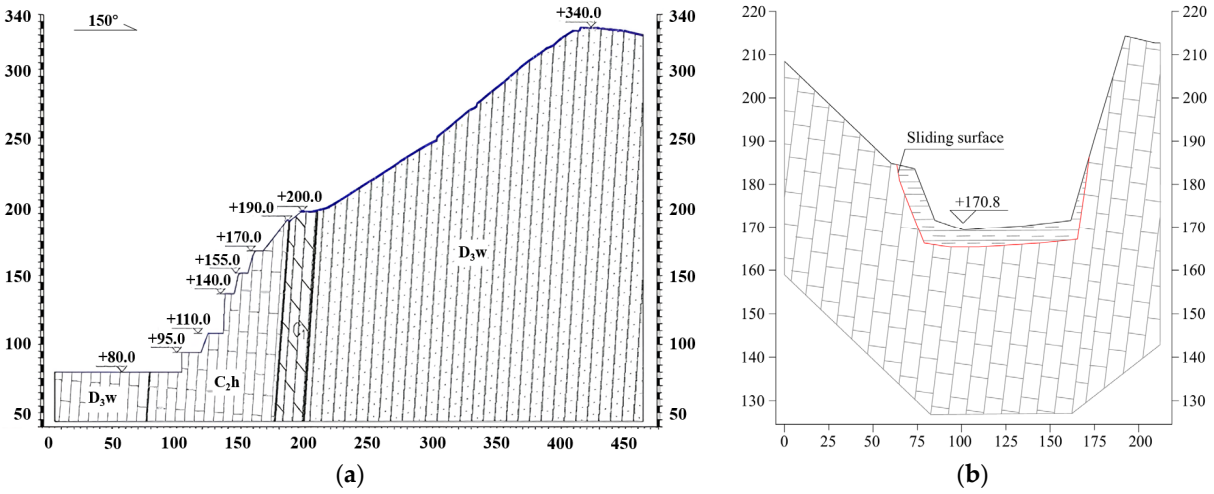


Figure 4. Diagram of the section map. (**a**) Longitudinal section map; (**b**) cross section map.

The overlying soil is affected by the slope cutting, leading to the traction landslide. Although the slope has a dual structure of rock and soil, the information revealed by borings and the prospecting trench on the rock–soil boundary (Figure 5) indicates that the rock–soil boundary is relatively gentle, with a low possibility of sliding and failure of the overlying soil layer along this surface. Meanwhile, the development of joints in the rock mass was revealed (Table 1). To verify the influence of the combination of structural planes on slope stability, the polar stereographic projection was adopted to determine the possibility of potential failure (Figure 6). The intersection lines of the structural plane (the rock layer, L_1, and L_2) have the opposite inclination to the slope surface, which verifies that the combination of the structural planes is a stable structure.

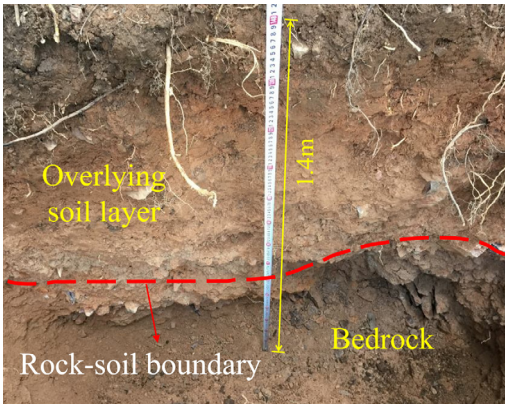


Figure 5. Prospecting trench on the rock–soil boundary.

Table 1. Dip direction and dip angle.

Number	Structure Type	Dip Direction (°)	Dip Angle (°)
P	slope surface	35	53
C	bedding plane	196	85
L_1	joint	330	70
L_2	joint	260	75

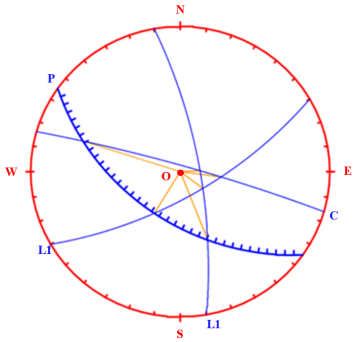


Figure 6. Diagram of equatorial projection.

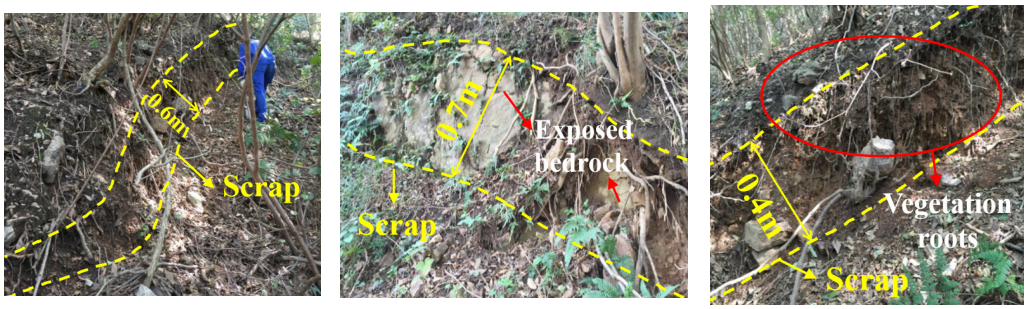
2.3. Deformation Characteristics and Materials Composition of the Landslide

According to the field investigation results and the information exposed by borings and prospecting trenches, the deformation characteristics and material composition of the landslide were determined.

2.3.1. Deformation Characteristics

The landslide is a small, shallow soil landslide with the volume of about 3.95×10^4 m^3, 0.8–2 m average thickness, 130 m average width, and 380 m average length, which has a clear perimeter and a tongue shaped distribution.

The deformation characteristics of the landslide are obvious in the trailing edge area (Figure 7), the front edge area (Figure 8), and the central area (Figure 9). After the landslide creep, the rear wall of the landslide is obvious (Figure 7a,b), while the bedrock and vegetation roots in the rear wall areas are exposed (Figure 7c). With the development of creep deformation, the deformation in the front part of the landslide gradually accumulated and accelerated under influencing factors, forming a tongue shaped sliding body at the step (Figure 8a,b); a grouted rubber retaining wall can be seen at the front edge of the landslide, where cracks, bulges, and stone detachment developed under the landslide thrust (Figure 8c). In the middle of the landslide, scraps formed along the slope due to tensile stress, with a height difference of no more than 1m (Figure 9a). Diverted trees are distributed on the surface of the Kong Mountain landslide (Figure 9b).



(**a**) (**b**) (**c**)

Figure 7. Deformation characteristics in trailing edge area. (**a**) Scarp; (**b**) exposed bedrock; (**c**) exposed vegetation roots.



(**a**) (**b**) (**c**)

Figure 8. Deformation characteristics in front edge area. (**a**) Diagram of slide tongue; (**b**) side view of slide tongue; (**c**) deformation of retaining wall.



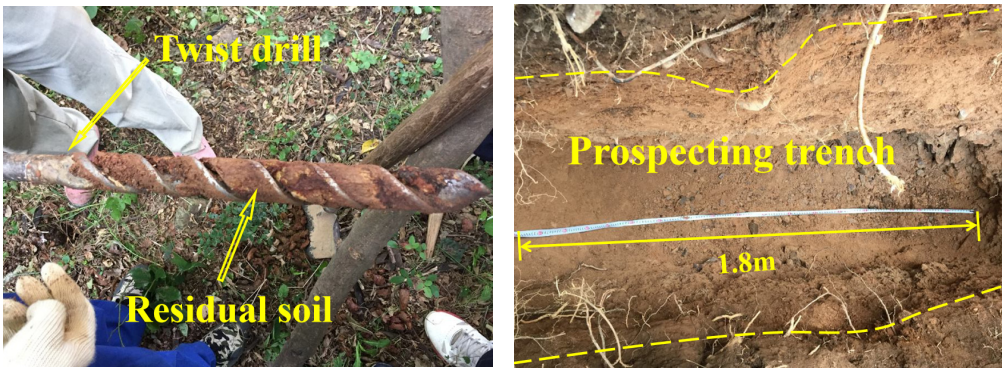
(**a**) (**b**)

Figure 9. Deformation characteristics in the central area. (**a**) Scarp; (**b**) diverted trees.

2.3.2. Materials Composition of the Kong Mountain Landslide

1. Sliding mass

According to the borings, prospecting trench and twist drill (Figure 10), the sliding mass is mainly composed of a large proportion of Quaternary residual soil (Q_4^{el}) and a small proportion of fill soil (Q^{ml}) with an average thickness of 0.8 m. The fill soil with uneven quality including silty clay, fragments, and weathered rock blocks, in which the particle size of hard fragments varies, generally ranging from 5 to 12 cm, and in some cases reaching 15 cm, 40 cm, and 80 cm. The yellowish-brown residual soil mainly consists of plastic silty clay, characterized by a smooth cutting surface and moderate dry strength and toughness. The silty clay is locally mixed with little sub-circular shaped, weathered, randomly arranged rock blocks.



(**a**) (**b**)

Figure 10. The residual soil revealed by: (**a**) twist drill; (**b**) prospecting trench.

2. Sliding zone

The residual soil, with strong permeability, developed vertical joints, and plant roots, provides favorable conditions for rainfall infiltration. The infiltrated water remains at the rock–soil boundary, forming a weak sliding surface. Based on the field investigation results, it can be concluded that the sliding zone is mainly located at the bottom of residual soil near the rock–soil boundary.

3. Sliding bed

Based on the field investigation and section map (Figure 4), it can be concluded that the sliding bed of the landslide from the upper to the lower consists of strongly to moderately weathered sandstone (D_{3w}), strongly to moderately weathered mudstone (C_{2h}), and strongly to moderately weathered limestone (C_2P_{1C}).

2.4. Analysis of Influencing Factors of Kong Mountain Landslide Stability

After the occurrence of the Kong Mountain landslide, the factors affecting its stability were analyzed based on the field investigation. The main influencing factors are as follows.

1. Topography

The height difference between the front edge and trailing edge of the landslide is about 108–134 m. The terrain is relatively steep while the slope angle is around 35°. Also, the middle and lower parts of the slope underwent slope cutting, leading to reduced landslide resistance. Therefore, the topography of the landslide provides sliding space for deformation.

2. Lithology

The sliding body is mainly composed of residual soil with silty clay where the rainfall is prone to infiltration. Due to the relatively poor permeability of the bedrock compared to the residual soil, rainwater retains at the rock–soil boundary, softening the lower part of the residual soil and accelerating the penetration of the shear sliding surface of the landslide.

3. Rainfall

Rainfall causes surface and subsurface erosion on both the landslide and slope, as well as inside the landslide body, leading to the soil collapse on the slope surface and the formation of dominant seepage channels within the landslide body. When the rainfall intensity is low, rainwater seeps into the shallow surface, increasing the moisture content of the sliding body and reducing the soil shear strength. With the increase in rainfall intensity, the moisture content further increases, and the soil shear strength further decreases, while the kinetic energy and runoff of rainwater increase, forming scouring ditches on the landslide surface. Due to the large catchment area of the Kong Mountain landslide located in the gully of the mine slope, most rainwater converges along the terrain to the landslide, accelerating the infiltration of rainwater and potentially causing secondary instability of the Kong Mountain landslide.

4. Human Engineering Activities

Early mining activities cut the slope, providing the terrain conditions for deformation of the overlying soil layer. Due to the shallow and low thickness, the residual slope soil continuously slides and collapses under external forces, reducing the anti-slip ability and leading to the expansion upwards to the trailing edge and the larger scope of landslide. Meanwhile, the disturbance caused by the construction of the slope reinforcement project will also have a certain impact on the stability of the Kong Mountain landslide.

2.5. Treatment Measures of Kong Mountain Landslide

The landslide is reinforced with round anti-slip piles and prestressed anchor cables. There are three rows of anti-slip piles. The piles (type A) in the 4th and 5th slope step have a diameter of 1.2 m, a length of 12 m, and a center distance of 3 m, while the anti-slip piles (type B) in the 6th slope step have a diameter of 1.8 m, a length of 15 m, and a center distance of 5 m. Also, prestressed anchor cables are set on the top face of the anti-slip piles. These cables are 35 m in length and made from 7Φs15.2 stranded wire. Owing to the fact that the system water interception and drainage can prevent the water and surface water infiltration as the effective mitigation measure, interception drains are set around the landslide boundary and slope steps, while the drainage drains are set across the sliding body. The treatment and drainage measures are shown in Figure 11.

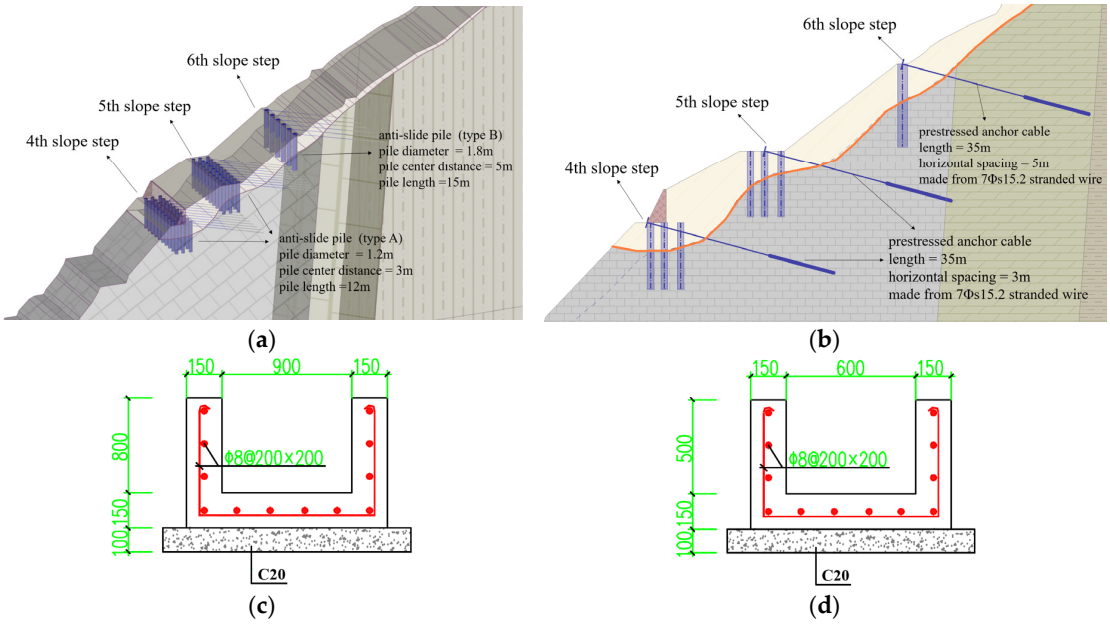


Figure 11. Treatment measures of Kong Mountain landslide. (**a**) Treatment measures shown in 3D model; (**b**) treatment measures shown in sectional drawing; (**c**) diagram of interception drain structure (mm); (**d**) diagram of drainage drain structure (mm).

3. Methodology

3.1. Two-Dimensional Finite Element Method and Improved Limit Equilibrium Method

The finite element method (FEM) can be utilized for stress, strain and seepage calculation of landslides to analyze the deformation and failure mechanisms and to clarify the areas prone to yield failure. The FEM reduces the shear strength on the sliding surface in the same proportion during the calculation process. When the landslide body reaches the ultimate equilibrium state along the sliding surface, it is considered a failure state, which can be expressed as Equations (1) and (2):

$$\int_0^l \tau dl = \int_0^l \left(\frac{c}{F_{sl}} + \sigma \frac{tan\varphi}{F_{sl}} \right) dl = \int_0^l \left(c' + \sigma tan\varphi' \right) dl \tag{1}$$

$$F_{sl} = \frac{\int_0^l (c + \sigma tan\varphi) dl}{\int_0^l \tau dl} \tag{2}$$

where τ is shear strength, l is the sliding surface length, c is the cohesion, φ is the internal friction angle, c' is the effective cohesion, φ' is the effective internal friction angle, F_{sl} is the reduction coefficient.

The analysis shows that the Kong Mountain landslide is mainly affected by rainfall. Due to the influence of rainfall on the changes in the pore water pressure inside the sliding body, the ordinary limit equilibrium method (LEM) is difficult to meet the requirements of landslide stability analysis. To take the changes of pore water pressure in the landslide under rainfall into consideration, the changes in pore pressure under unstable seepage is incorporated into the existing LEM, according to the slope's geometric model under seepage conditions.

The pore water pressure inside the landslide can be divided into static pore water pressure and excess pore water pressure. Due to the fact that the pore water pressure in a stable seepage field does not change with time and is generated by the weight of water, it belongs to static pore water pressure. The excess static pore water pressure is generally generated under additional stress and influenced by the pore pressure coefficient, which affects the soil slope stability. The pore pressure coefficient is the ratio of excess pore pressure increment to total stress increment when the fluid in the soil cannot freely enter and exit. The static pore water pressure can be expressed as Equation (3) while the excess pore water pressure can be expressed as Equations (4) and (5):

$$u_a = h \times \gamma_w \tag{3}$$

$$\Delta u = \Delta u_1 + \Delta u_2 = B[\Delta\sigma_3 + A\Delta(\sigma_1 - \sigma_3)] \tag{4}$$

$$B = \frac{1}{1 + n\frac{C_f}{C_{sk}}} \tag{5}$$

where u_a is the static pore water pressure, h is the height, γ_w is the buoyant density of soil mass, Δu is the excess pore water pressure, B is the pore water pressure coefficient under isotropic conditions, A is the pore water pressure coefficient under the influence of deviational stress increment, C_f is the the volume compression coefficient of the pore fluid, and C_{sk} is the volume compression coefficient of the soil skeleton.

Under stable seepage, the soil inside the landslide has completely consolidated under weight, but the rainfall causes an increase in the excess pore water pressure on the sliding surface. Therefore, the principle of effective stress can meet the needs of soil slope stability analysis under seepage action. Assuming point b in the soil slope is the center point of a certain block of ground, and point a is the intersection point of the equipotential line

passing through point b and the groundwater level, the pore water pressure at point b under seepage is the head difference between points a and b (Figure 12). If buoyant density is applied to the soil below the water surface outside the slope, the pore water pressure caused by stable seepage can be expressed as Equation (6):

$$u_i = h_{wi} \times \gamma_w \tag{6}$$

where u_i is the pore water pressure under stable seepage, h_{wi} is the height difference between point a and the extending water surface, and γ_w is the water density.

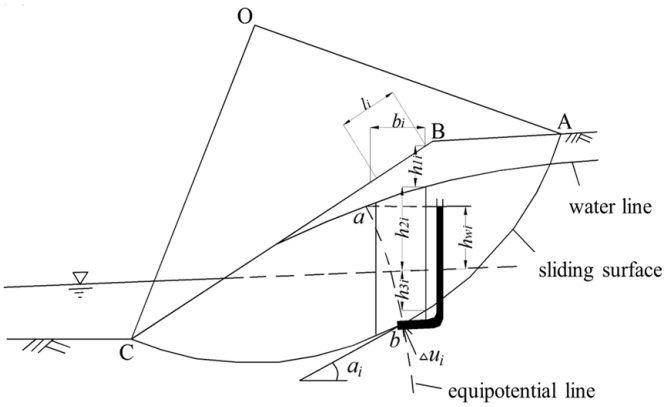


Figure 12. Diagram of soil slope stability calculation under seepage action.

The increase in pore water pressure is higher under unstable seepage conditions compared to stable seepage conditions, which can be represented as Δu_i with the direction of action pointing towards the circle center. Therefore, the LEM has been improved to analyze the landslide stability under unstable seepage, which can be expressed as Equation (7):

$$F_s = \frac{\sum c' l_i + \sum [b_i(\gamma h_{1i} + \gamma' h_{2i} + \gamma' h_{3i})cos\alpha_i - h_{wi}\gamma_w b_i sec\alpha_i - \Delta u_i l_i]tan\varphi'}{\sum b_i(\gamma h_{1i} + \gamma_{sat} h_{2i} + \gamma' h_{3i})sin\alpha_i} \tag{7}$$

where F_s is the stability coefficient, c' is the effective cohesion, l_i is the arc length, b_i is the slice width, h_{1i} is the height of the natural soil mass, h_{2i} is the height of the soil mass between the water line and the extending water surface, h_{3i} is the height of the soil mass between the extending water surface and the sliding surface, α_i is the angle of the soil slice, and γ, γ' and γ_{sat} are the natural, buoyant, and saturated density of the soil, respectively.

According to the typical section, the 2D model (Figure 13) is established for calculation using the couple method of the finite element method and the improved limit equilibrium method (FEM–LEM) for stability calculation. The boundary conditions of the 2D model have been set as the impermeable bottom boundary, the pore water pressure left and right boundaries, and the infiltration slope boundary under steady seepage conditions, while the discharge outlets are set for the slope boundary under unsteady seepage conditions. The Van-Genuchten model (VG model) is adopted for the rock and soil mass. To determine the influence of steady and unsteady seepage on pore water pressure changes and the slope stability under the rainfall conditions more realistically, the couple method of FEM–LEM is carried out by importing the improved LEM into finite element software through an interface. The FEM software (GEO5 2022) can simulate the distribution of the pore water pressure inside the landslide by setting the initial pore water pressure, the rainfall conditions, the seepage parameters, etc. according to the unsaturated soil mechanics, which can be combined with the improved LEM to calculate the slope stability coefficient.

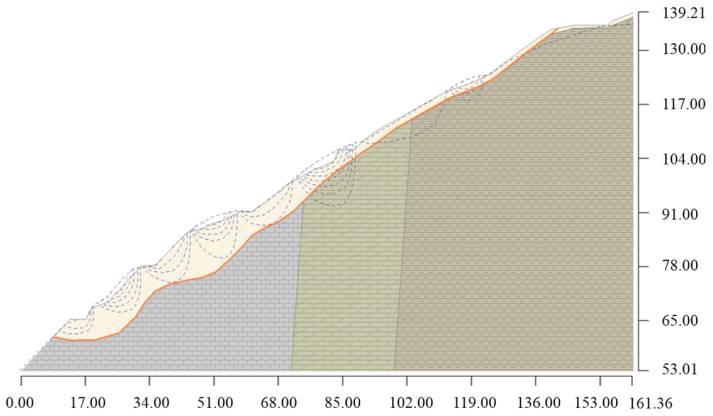


Figure 13. The computational model for two-dimensional calculation.

3.2. Calculation Theory of FLAC 3D and Three-Dimensional Model Establishment

FLAC 3D 6.0 is a software that represents the motion of nodes using finite difference in the computational model. It calculates the strain of the element based on node velocity, and the stress of elements using the stress–strain relationship, ultimately solving the nodes' velocity and displacement through the equilibrium equation. The calculation iterates and loops continuously until all calculation areas reach convergence, thereby accurately simulating the deformation and failure of the Kong Mountain landslide. In this study, FLAC 3D 6.0 was used to calculate the results such as stress, strain, displacement, etc. of the landslide to analyze the stability changes under the different working conditions.

The calculation model of Kong Mountain landslide was established based on the typical section, consisting of sandstone, mudstone, limestone and the sliding mass. The model dimensions are 270 m (length) × 32 m (width) × 270 m (height), and it includes 15,965 nodes and 79,780 grid cells (Figure 14). In the model, the Mohr–Coulomb model is set for the rock and soil mass, the boundary conditions are set to limit the deformation and stress, and the pile structural units and the cable structural units are adopted for the anti-sliding piles and the prestressed anchor cables, respectively. The initial crustal stress generated by gravity is set inside the model, while the vertical stress is converted by gravity and the horizontal stress is taken as 0.5 times of the vertical stress. To implement the rainfall conditions and realize the unsaturated seepage in FLAC 3D, the FISHCALL command of the FISH functions are applied to automatically adjust the FISH and FLAC3D variables, such as mechanical parameters and seepage parameters, which can calculate the increment of saturation by calculating the changes of the fluid volume variations in nodes, while the permeability coefficient of the unsaturated zone is calculated based on the relationship between saturation and negative pressure.

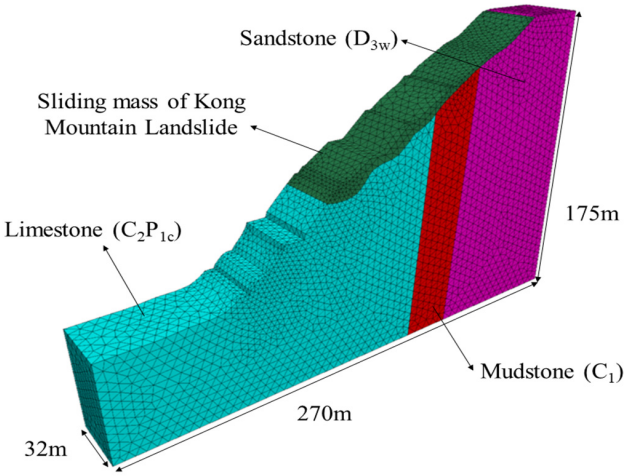


Figure 14. Calculation of geological model of the Kong Mountain landslide.

3.3. Rock and Soil Calculation Parameters

The rock layers of the mining slope are limestone, mudstone, and sandstone, while the sliding mass is mainly composed of Quaternary residual soil. The values of the friction and cohesion for the rock and soil mass are selected based on the laboratory test results and in situ test data [36,37], while other parameters are comprehensively adopted according to the related standards [38–40], Hoek–Brown empirical parameters, and other similar projects near the study area. The specific calculation parameters of rock mass and soil mass used for calculation are shown in Table 2.

Table 2. Calculation parameters of rock and soil mass for calculation.

Lithology	Weight (kN/m^3)		c (kPa)		φ (°)		Deformation Modulus/E	Poisson's Ratio/μ	Permeability Coefficient/k	Initial Void Ratio/e_0
	Naturally	Saturation	Naturally	Saturation	Naturally	Saturation	MPa	/	m/d	/
Limestone	27.2	28.0	50.0	45.0	20.0	15.0	7.5×10^4	0.17	5.2×10^{-2}	0.56
Mudstone	23.0	24.0	30.0	24.0	18.0	15.0	4×10^3	0.4	1.7×10^{-4}	0.11
Sandstone	25.0	26.0	42.0	38.0	29.0	24.4	3×10^3	0.2	2.6×10^{-3}	0.25
Sliding Mass	19.0	20.0	15.0	12.0	22.5	18.5	30	0.3	1.2	0.18
Sliding Zone	19.0	20.0	14.0	9.0	19.5	14.5				

4. Research Results

4.1. Analysis of Calculation Results of Two-Dimensional Numerical Simulation

4.1.1. Analysis of Pore Water Pressure Distribution on the Landslide of Different Rainfall and Seepage Conditions

To further clarify the influence of different rainfall and seepage conditions on the pore water pressure changes, the study further refined rainfall working conditions by setting different rainfall intensities and durations according to the rainfall characteristics in the study area. The seepage conditions include steady and unsteady seepage, the rainfall intensities consist of light rain (10 mm/d), moderate rain (45 mm/d), and heavy rain (90 mm/d). The rainfall durations considered are 2.5 h, 12 h, and 24 h. Also, the results with discharge outlets or not are compared to illustrate the influence of drainage conditions on the distribution of pore water pressure.

The pore water pressure distribution under different rainfall and seepage conditions on the landslide is simulated using the FEM software. The distribution of pore water pressure under steady seepage conditions is shown in Figure 15, while the distributions under unsteady seepage without discharge outlets and with several discharge outlets are shown in Figures 16 and 17, respectively.

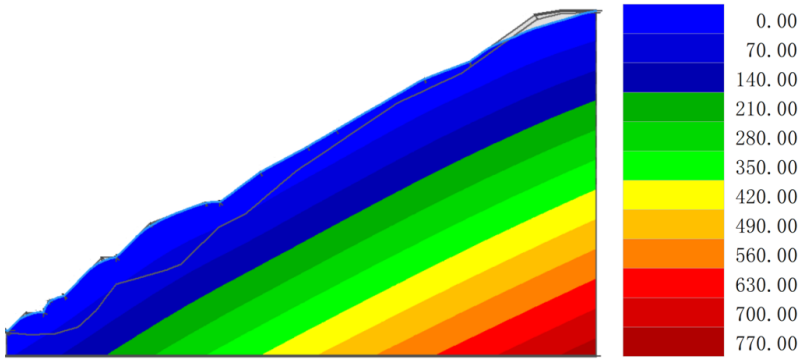


Figure 15. The distribution of pore water pressure under steady seepage (kPa).

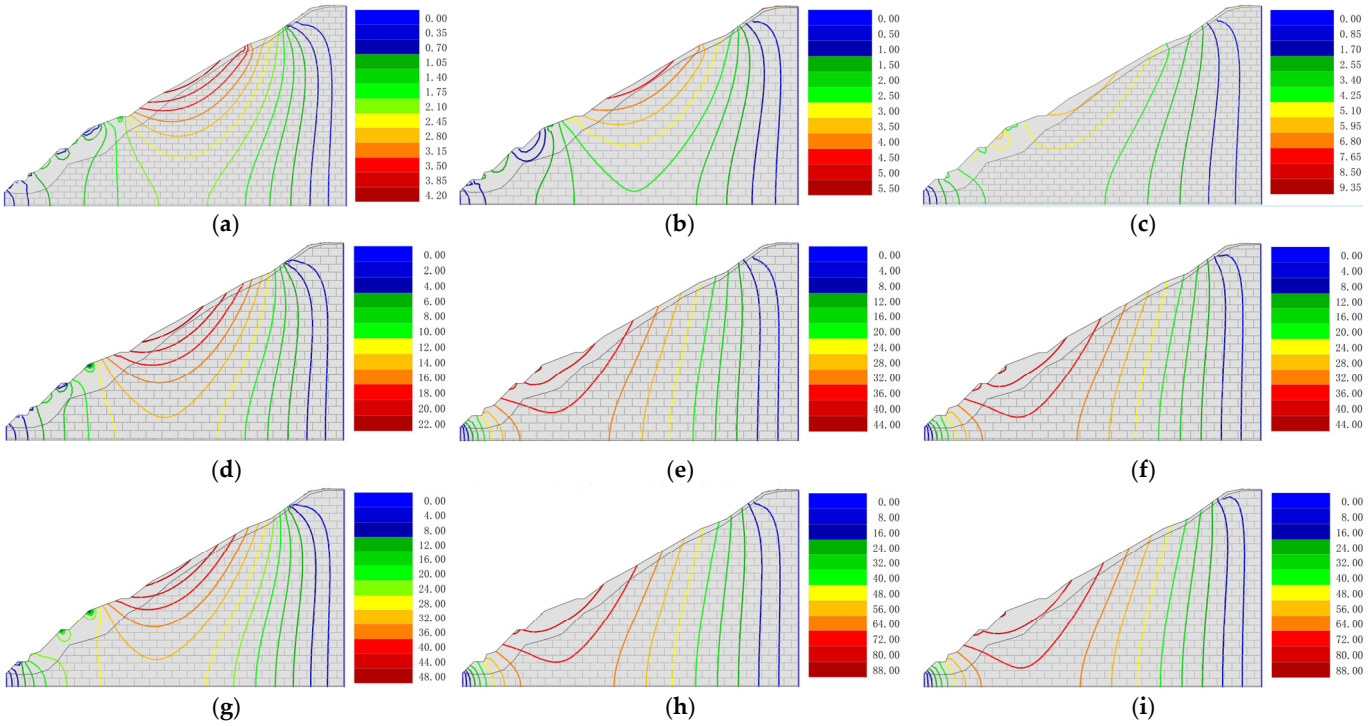


Figure 16. The distribution of pore water pressure under unsteady seepage with no discharge outlet (kPa). (**a**) Light rain + 2.5 h; (**b**) light rain + 12 h; (**c**) light rain + 24 h; (**d**) moderate rain + 2.5 h; (**e**) moderate rain + 12 h; (**f**) moderate rain + 24 h; (**g**) heavy rain + 2.5; (**h**) heavy rain + 12 h; and (**i**) heavy rain + 24 h.

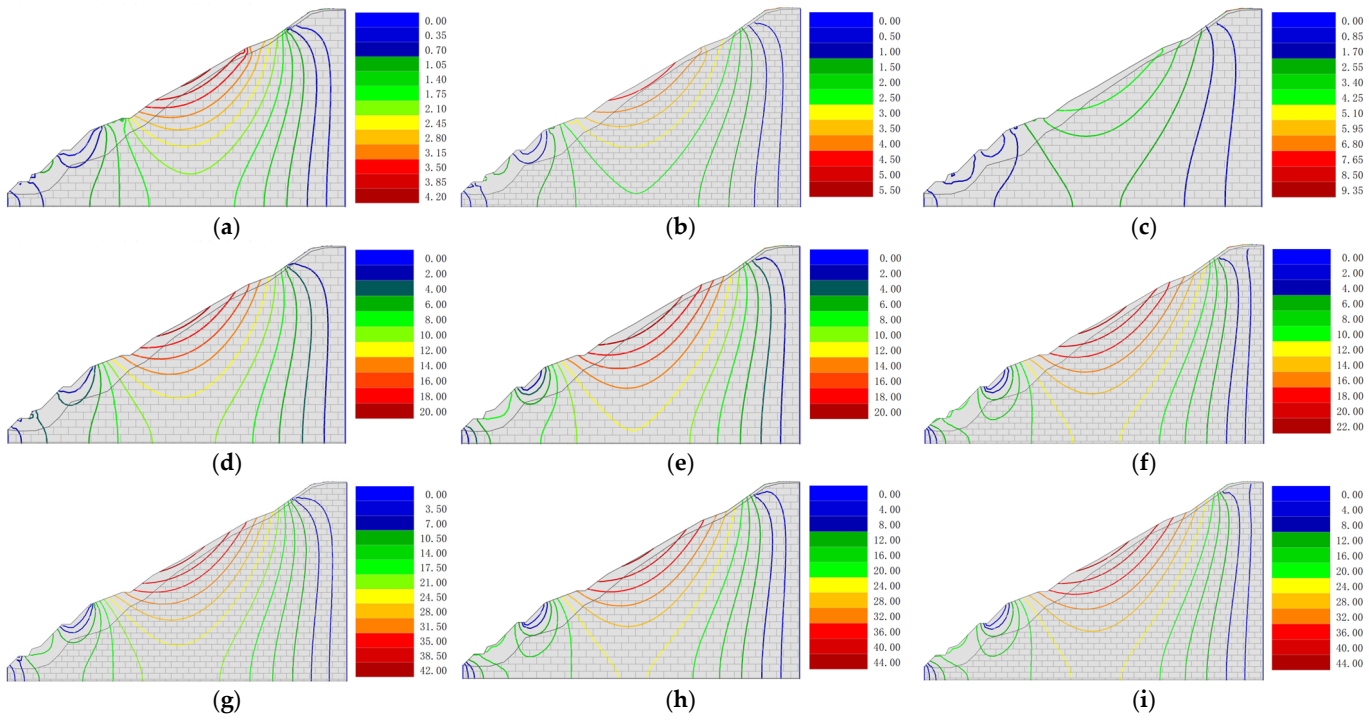


Figure 17. The distribution of pore water pressure under unsteady seepage with discharge outlets (kPa). (**a**) Light rain + 2.5 h; (**b**) light rain + 12 h; (**c**) light rain + 24 h; (**d**) moderate rain + 2.5 h; (**e**) moderate rain + 12 h; (**f**) moderate rain + 24 h; (**g**) heavy rain + 2.5 h; (**h**) heavy rain + 12 h; and (**i**) heavy rain + 24 h.

According to the calculation results of the distribution of the pore water pressure inside the landslide, as shown in Figures 16 and 17, the following can be seen:

1. Under the different rainfall intensities and durations, the pore water pressure in the landslide increased proportionally with depth in both steady and unsteady seepage conditions.
2. When the rainfall intensity is light, there is little difference in the distribution of pore water pressure, regardless of whether there are discharge outlets under the same rainfall intensity.
3. Under moderate and heavy rain conditions, there is little difference under different discharge conditions with the 2.5 h rainfall duration, while the pore water pressure increment with discharge outlets is around 1/2 of that with no discharge outlet.
4. Comparing the simulation results of the pore water pressure under the 12 h and 24 h rainfall durations, the water pressure distribution is basically consistent although the maximum pore water pressure keeps increasing in each discharge condition.

Therefore, based on the simulation results and analysis, it can be concluded that water discharge can reduce the pore pressure after a certain period of time. Also, continuous rainfall will not cause a sustained increase in pore water pressure when the rainfall duration reaches a certain value.

4.1.2. Analysis of Plastic Zone of Kong Mountain Landslide

The plastic zone of a typical section of the landslide is calculated under the most unfavorable rainfall condition, with 90 mm/d rainfall intensity and 2.5 h rainfall duration, by the FEM software (Figure 18).

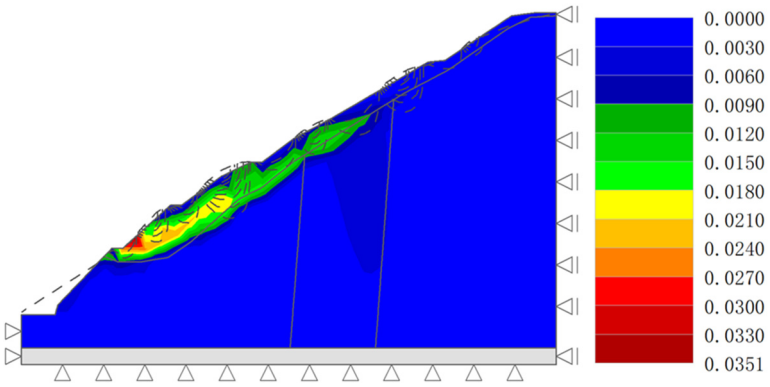


Figure 18. The plastic zone of a typical section of Kong Mountain landslide.

After the shallow soil mass of the residual soil reached a saturation state, the rainwater on the slope surface migrated to the slope foot under gravity after a period of rainfall, resulting in the formation of a transient saturation zone at the slope foot. As shown in Figure 18, the plastic zone inside the slope is mainly concentrated at the front edge and foot of the landslide, which is basically consistent with the potential sliding surface determined by the field investigation and drillings, making it relatively dangerous. Therefore, the deformation characteristics revealed by the field investigation show that the Kong Mountain landslide is in the creep stage, and the possibility of the run-through of the plastic zone is high under the unsteady seepage condition.

4.1.3. Analysis of Stability Coefficient of Kong Mountain Landslide

The stability coefficient results of the Kong Mountain landslide under different working conditions have been calculated by both the FEM and the coupled FEM–LEM method, respectively. The evaluation standards of the stability judgment are adopted based on the code for the design of landslide stabilization [41]. The calculation results and evaluation standards are shown in Table 3.

Table 3. Calculation results of the stability of the Kong Mountain landslide via FEM and FEM–LEM.

Working Condition	Standards of the Stability Judgement	Stability Coefficient	
		FEM	FEM–LEM
Natural	1.30	1.07	1.03
Rainfall	1.25	1.01	0.95

According to the calculation results, the following can be concluded based on the deformation characteristics and the qualitative analysis results:

1. The stability of the Kong Mountain landslide can not meet the need of the safety requirements under natural and rainfall working conditions according to the calculation result of both calculation methods.
2. There is a certain difference in the stability coefficient of the Kong Mountain landslide of the two calculation methods; that is, the calculation result of FEM is greater than that of FEM–LEM. The FEM calculation results indicate that the landslide is in a basically stable state under natural working conditions, with a stability coefficient of 1.07, and in an under-stable state under rainfall working conditions, with a stability coefficient of 1.01. However, the results of the FEM–LEM indicate that the landslide is in an under-stable state under natural working conditions, with a stability coefficient of 1.03, and in an unstable state under rainfall working conditions, with a stability coefficient of 0.95.
3. The results of the FEM–LEM are closer to the actual situation compared with the deformation characteristics, which impacts the changes in pore water pressure and corresponds to the analysis that the increase in rainfall accelerates the changes in pore water pressure and the instability of landslides.
4. Since the stability of the landslide does not meet safety requirements, disturbances caused by human engineering activities may lead to further landslide deterioration. Therefore, systematic treatment measures are needed to improve landslide stability.

4.2. Analysis of Calculation Results of Three-Dimensional Numerical Simulation

The two-dimensional numerical simulation results indicate that pore water pressure plays a critical role in landslide stability and treatment measures are needed. Therefore, to verify the effectiveness of treatment measures under the impact of pore water pressure, a three-dimensional numerical simulation by FLAC 3D 6.0 is used for calculation of the landslide with or without reinforcement, and the results such as the displacement, plastic zone, etc. under different working conditions are compared. Four working conditions were considered in the three-dimensional numerical simulation:

1. Working condition 1: natural working condition;
2. Working condition 2: rainfall working condition (90 mm/d rainfall intensity and 2.5 h rainfall duration)
3. Working condition 3: working condition 1 + treatment measures;
4. Working condition 4: working condition 2 + treatment measures.

4.2.1. Analysis of the Displacement and Stability Coefficient of the Kong Mountain Landslide under Different Working Conditions

The calculation results of displacement under different working conditions are shown in Figure 19. The calculation result of natural working conditions is the basis for subsequent calculations.

According to Figure 19, the following can be concluded according to the cloud maps of the displacement:

1. Regardless of whether there are treatment measures, deformation is mainly concentrated in the landslide area, especially on the surface of the landslide. The maximum displacement under rainfall conditions (0.274 for working condition 2 and 0.016 for working condition 4) is higher than under natural conditions (0.012 for working con-

dition 1 and 0.009 for working condition 3), which is mainly affected by the increase in self-weight and pore water pressure under rainfall.

2. The stability coefficients of the Kong Mountain landslide under each working condition are 1.02, 0.94, 1.38, and 1.31, respectively, which indicates that the treatment measures can improve the landslide stability effectively. The reduction of displacement value after the application of the treatment measures also explains the effectiveness of treatment measures.
3. The area with the obvious displacement is basically consistent with the plastic zone obtained by the FEM–LEM, indicating the applicability of the FEM–LEM considering the changes in pore water pressure.

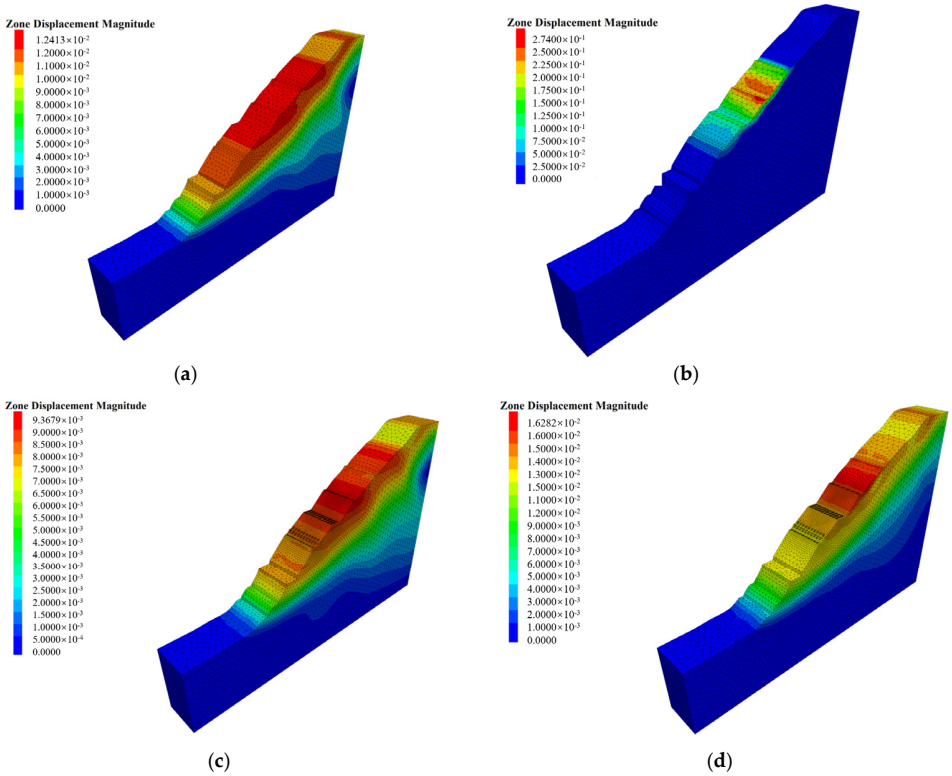


Figure 19. The cloud maps of the displacement under different working conditions: (**a**) working condition 1; (**b**) working condition 2; (**c**) working condition 3; (**d**) working condition 4.

Therefore, combined with the displacement cloud map, it can be concluded that the rainfall infiltration leads to the rapid saturation of shallow part of the landslide and the increase in pore water pressure. In addition, the landslide is located in the watershed area of the mining slope so that the deformation cracks and scraps on the landslide accelerated the infiltration of rainwater when the rainwater collects in the landslide area, which may ultimately lead to deformation.

4.2.2. Analysis of the Shear Strain and the Plastic Zone of the Kong Mountain Landslide Under Different Working Conditions

The maximum shear strain and distribution of the plastic zone under different working conditions are shown in Figures 20 and 21. According to Figures 20 and 21, it can be summarized that the shear strain is mainly located on the deep part of the slope and the maximum value is concentrated at the foot of the slope under working conditions 1 and 3. The whole slope is mainly subjected to shear deformation while there is little tension deformation on the slope surface. The plastic zone has not yet fully connected to the deep part of the slope. So, the stability of the whole slope is stable and the possibility of deep sliding is low, which is consistent with the analysis results of the potential sliding models and the field investigation results.

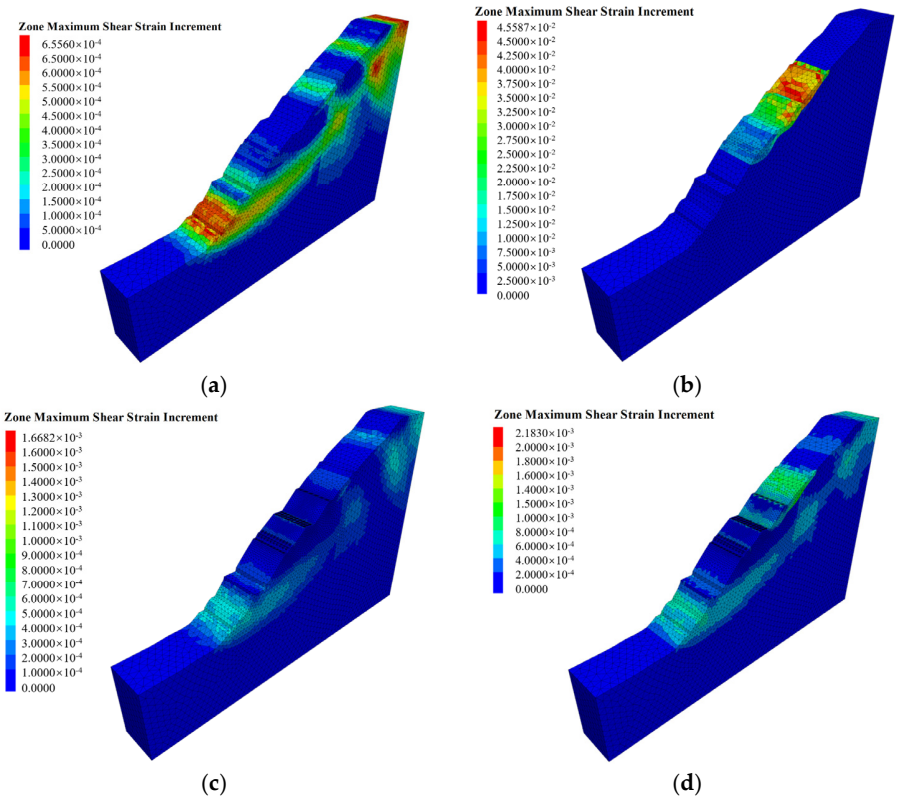


Figure 20. The cloud maps of the maximum shear strain under different working conditions: (**a**) working condition 1; (**b**) working condition 2; (**c**) working condition 3; (**d**) working condition 4.

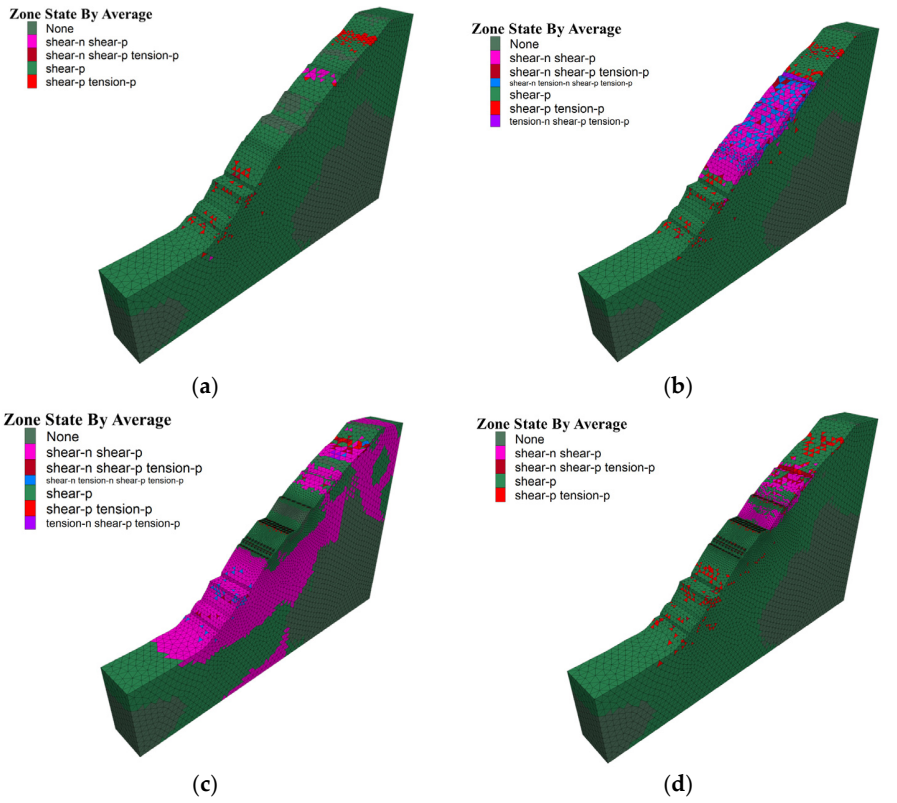


Figure 21. The plastic zone under different working conditions: (**a**) working condition 1; (**b**) working condition 2; (**c**) working condition 3; (**d**) working condition 4.

However, the concentration of the shear strain appeared on the sliding mass under rainfall (under working conditions 2 and 4). Under working condition 2, the maximum shear strain value is mainly on the slope surface where the plastic zone concentrates show that the sliding mass undergoes the shear deformation and tension deformation at the same time.

According to the simulation results of the displacement, shear strain and plastic zone with or without treatment measures, it can be concluded that the treatment measures are able to effectively reduce the tension and shear deformation and control the development of the landslide deformation. The Kong Mountain landslide after reinforcement is shown in Figure 22.



(**a**) (**b**)

Figure 22. The Kong Mountain landslide after treatment: (**a**) side view; (**b**) front view.

5. Discussion

The paper studied the impact of pore water pressure on landslide stability and verified the effectiveness of treatment measures according to the results of two-dimensional and three-dimensional numerical simulations. Through the analysis, the following can be drawn:

1. The main influence factor of the landslide deformation is the changes of the pore water pressure inside the sliding mass under rainfall. Also, the location, discharge condition, and composition of the Quaternary residual soil provide conditions of rainfall infiltration. So, under rainfall, the soil mass of the landslide with strong permeability undergoes a further reduction in shear strength, which leads to the deformation and failure of the Kong Mountain landslide directly.
2. The existence of deformation characteristics on the landslide, such as scraps, exposed bedrock, exposed vegetation roots, diverted trees, etc. provide convenience for the infiltration of more rainwater and surface runoff. The deformation will be the expanding location of further destruction once the sliding force caused by external effects is greater than the critical value that it can withstand.
3. The cutting slope without reinforcement can only meet the stability requirements during the mining process and the vegetation can not totally stop the rainwater infiltration. According to the calculation results of the numerical simulation, the treatment measures can effectively control the development of the landslide deformation. Therefore, specific treatment measures for the landslide should include reinforcement with anti-slip piles and prestressed anchor cables, along with system water interception and drainage measures.

However, although the study discussed the landslide stability under rainfall and verified the effectiveness of the specific treatment measures, there are some limitations within the discussion and the simulation. Firstly, there are some similarities between the 2D and 3D simulations, such as the plastic zone distribution. Although different simulations can provide mutual verification and reference based on different theories, the

simulation content can be expanded by exploring different perspectives. Additionally, the matrix suction, negative pore pressure, and dynamic pore pressure, all of which can affect landslide stability, are not well discussed in the study. Therefore, in a subsequent study, the simulation and analysis of the matrix suction, negative pore pressure, and dynamic pore pressure should be further discussed. Moreover, the related parameters used in the simulation are comprehensively selected from the laboratory test reports, related engineering projects, and their related standards and criteria. To make the calculation parameters more accurate, more laboratory tests should be taken.

6. Conclusions

In the study, the deformation characteristics and influencing factors of landslides are clarified through field investigation results. The FEM–LEM and the FLAC 3D were used to simulate the water pore pressure, plastic zone, displacement, etc., evaluate the stability of the Kong Mountain landslide, and verify the effectiveness of treatment measures. The conclusions can be drawn as follows:

1. The excavated slope is stable after mining activities, but the Kong Mountain landslide is undergoing deformation with few signs of deformation under the natural working conditions.
2. The rainfall infiltration within the sliding mass accelerates the weakening process of the landslide, which leads to the reduction of soil shear strength. The permeability coefficient of the sliding bed is relatively lower so that the rainwater collects on the soil–rock boundary, causing the form of the sliding zone.
3. The improved LEM was proposed and the simulation using the FEM–LEM was conducted to prove the impact of the pore water pressure on the landslide stability under rainfall. There is little difference between the calculation results of the FEM–LEM with those of the FEM and FLAC 3D software, which verified the applicability of the improved LEM for landslide stability.
4. According to the cloud map of the plastic zone, displacement, and the maximum shear strain, it can be concluded that the application of the anti-slip piles and the prestressed anchor cables can improve the stability of the landslide by effectively controlling the landslide deformation development and limiting the plastic zone.

Author Contributions: Conceptualization, L.T. and Y.Y. (Yun Yan); methodology, F.Z. and Y.Y. (Yuru Yan); software, X.L., H.Z. and X.Z.; validation, Y.L. and F.Z.; visualization, Y.Y. (Yuru Yan) and Y.L.; investigation, L.T. and Y.Y. (Yun Yan); writing—original draft preparation, X.L., H.Z. and L.T.; writing—review and editing, X.L., X.Z. and L.T. All authors have read and agreed to the published version of the manuscript.

Funding: This research was funded by Jiangsu Provincial Geological Exploration Fund Project [2021-No.46] and Basic Research Special Funds of East China Exploration Bureau of Nonferrous Metals in Jiangsu Province (HDYS-KY2019-03).

Data Availability Statement: The data presented in this study are available on request from the corresponding author.

Conflicts of Interest: The authors declare no conflicts of interest.

References

1. Li, Y.; Xu, W.Y.; Wang, S.N.; Wang, H.L.; Dai, Y.X. Slope stability analysis with reference to rainfall infiltration in the Yongping Copper Mine, China. *Curr. Sci.* **2019**, *116*, 536–543. [CrossRef]
2. Zhao, L.; You, G. Rainfall affected stability analysis of Maddingley Brown Coal eastern batter using Plaxis 3D. *Arab. J. Geosci.* **2020**, *13*, 1071. [CrossRef]
3. Ma, G.T.; Hu, X.W.; Yin, Y.P.; Luo, G.; Pan, Y.X. Failure mechanisms and development of catastrophic rockslides triggered by precipitation and open-pit mining in Emei, Sichuan, China. *Landslides* **2018**, *15*, 1401–1414. [CrossRef]
4. Lu, Y.; Jin, C.Y.; Wang, Q.; Li, G.; Han, T. Deformation and failure characteristic of open-pit slope subjected to combined effects of mining blasting and rainfall infiltration. *Eng. Geol.* **2024**, *331*, 107437. [CrossRef]

5. McQuillan, A.; Canbulat, I.; Oh, J. Methods applied in Australian industry to evaluate coal mine slope stability. *Int. J. Min. Sci. Technol.* **2020**, *30*, 151–155. [CrossRef]
6. Faramarzi, L.; Zare, M.; Azhari, A.; Tabaei, M. Assessment of rock slope stability at Cham-Shir Dam Power Plant pit using the limit equilibrium method and numerical modeling. *Bull. Eng. Geol. Environ.* **2017**, *76*, 783–794. [CrossRef]
7. Zhao, X.D.; Zhao, Y.F.; Yu, W.L. The safety factor of a heterogeneous slope in an open-pit metal mine: A case study from the Tanjianshan gold mine. *Front. Earth Sci.* **2023**, *10*, 990454. [CrossRef]
8. Su, P.D.; Qiu, P.; Liu, B.; Chen, W.L.; Su, S.F. Stability prediction and optimal angle of high slope in open-pit mine based on two-dimension limit equilibrium method and three-dimension numerical simulation. *Phys. Chem. Earth* **2022**, *127*, 103151. [CrossRef]
9. Cao, H.; Ma, G.T.; Liu, P.; Qin, X.S.; Wu, C.P.; Lu, J. Multi-Factor Analysis on the Stability of High Slopes in Open-Pit Mines. *Appl. Sci.* **2023**, *13*, 5940. [CrossRef]
10. Renani, H.F.; Martin, C.D. Factor of safety of strain-softening slopes. *J. Rock Mech. Geotech. Eng.* **2020**, *12*, 473–483. [CrossRef]
11. Shang, L.; Nguyen, H.; Bui, X.N.; Vu, T.H.; Costache, R.; Hanh, L.T.M. Toward state-of-the-art techniques in predicting and controlling slope stability in open-pit mines based on limit equilibrium analysis, radial basis function neural network, and brainstorm optimization. *Acta Geotech.* **2022**, *17*, 1295–1314. [CrossRef]
12. Bar, N.; Kostadinovski, M.; Tucker, M.; Byng, G.; Rachmatullah, R.; Maldonado, A.; Poetsch, M.; Gaich, A.; McQuillan, A.; Yacoub, T.; et al. Rapid and robust slope failure appraisal using aerial photogrammetry and 3D slope stability models. *Int. J. Min. Sci. Technol.* **2020**, *30*, 651–658. [CrossRef]
13. Di, B.F.; Stamatopoulos, C.A.; Stamatopoulos, A.C.; Liu, E.N.; Balla, L. Proposal, application and partial validation of a simplified expression evaluating the stability of sandy slopes under rainfall conditions. *Geomorphology* **2021**, *395*, 107966. [CrossRef]
14. Lambe, T.W.; Whitman, R. Soil stability with flow. In *Soil Mechanics*; John Wiley and Sons: New York, NY, USA, 1969.
15. Take, W.A.; Bolton, M.D.; Wong, P.C.P.; Yeung, F.J. Evaluation of landslide triggering mechanisms in model fill slopes. *Landslides* **2004**, *1*, 173–184. [CrossRef]
16. Nian, G.Q.; Chen, Z.H.; Bao, M.; Zhang, L.F.; Zhou, Z.H. Rainfall infiltration boundary conditions and stability of a fractured-rock slope based on a dual-continuum model. *Hydrogeol. J.* **2022**, *30*, 829–847. [CrossRef]
17. Zhang, L.F.; Chen, Z.H.; Tang, Y.S. Study on regional sliding failure modes and evolution regularity of slopes with weak layers. *Chin. J. Rock Mech. Eng.* **2021**, *40*, 1145–1154. (In Chinese) [CrossRef]
18. Qin, H.; Tang, H.; Yin, X.T.; Cheng, X. Disturbed zone calculation and stability evaluation method of footwall slope with slip-shear failure under excavation. *J. Cent. South Univ.* **2024**, *31*, 589–601. [CrossRef]
19. Zhao, J.J.; Li, J.S.; Ma, Y.T.; Yu, J.L. Experimental study on failure process of mining landslide induced by rainfall. *J. China Coal Soc.* **2020**, *45*, 760–769. (In Chinese) [CrossRef]
20. Li, X.S.; Li, Q.H.; Wang, Y.M.; Liu, W.; Hou, D.; Zheng, W.B.; Zhang, X. Experimental study on instability mechanism and critical intensity of rainfall of high-steep rock slopes under unsaturated conditions. *Int. J. Min. Sci. Technol.* **2023**, *33*, 1243–1260. [CrossRef]
21. Wang, W.C.; Li, J.P.; Wang, C.Y.; Chen, S.J.; Wang, P. Analysis of failure mode and deformation evolution characteristics of slopes under the influence of highwall mining. *Coal Sci. Technol.* **2023**, *51*, 321–336. (In Chinese) [CrossRef]
22. Tao, Z.G.; Zhang, T.X.; Zhu, D.Y.; Gong, W.L.; He, M.C. Physical Modeling Test on Deformation and Failure of Rock Slope with New Support System. *Adv. Civ. Eng.* **2020**, *2020*, 8825220. [CrossRef]
23. Wu, T.Y.; Zhou, C.B.; Jiang, N.; Xia, Y.Q.; Zhang, Y.Q. Stability analysis for high-steep slope subjected to repeated blasting vibration. *Arab. J. Geosci.* **2020**, *13*, 828. [CrossRef]
24. Mikroutsikos, A.; Theocharis, A.I.; Koukouzas, N.C.; Zevgolis, I.E. Slope stability of deep surface coal mines in the presence of a weak zone. *Geomech. Geophys. Geo-Energy Geo-Resour.* **2021**, *7*, 1056–1071. [CrossRef]
25. Wijesinghe, D.R.; Dyson, A.; You, G.G.; Khandelwal, M.; Natarajan, S.; Chan, A.D.; Ooi, E.T. Slope stability analysis considering fully saturated poro-elasto-plasticity by an image-based scaled boundary finite element approach. *Eng. Anal. Bound. Elem.* **2024**, *158*, 160–181. [CrossRef]
26. Sun, S.W.; Yang, Z.X.; Pang, B.; Hu, J.B.; Zhong, X.Y. Failure characteristics and mechanism of a landslide in weathered phyllite at Anqian iron mine, Liaoning, China. *Bull. Eng. Geol. Environ.* **2022**, *81*, 425. [CrossRef]
27. Chandra, V.S.J.; Panchal, S.; Sirdesai, N.N. Effect of Coal Seam Presence In-Between Comparatively Denser Layers Over High Wall Slope Stability-A Case Study of Kistaram Project, Singareni Collieries Company Limited (SCCL). *J. Geol. Soc. India* **2023**, *99*, 338–344. [CrossRef]
28. Yang, Z.A.; Liu, X.; Qian, W.M.; Ding, X.H.; Ao, Z.C.; Zhang, Z.Y.; Jiskani, I.M.; Tian, Y.; Xing, B.K.; Wahab, A. Investigation of Steep Waste Dump Slope Stability of Iron Ore Mine-A Case Study. *Appl. Sci.* **2024**, *14*, 3430. [CrossRef]
29. Peng, C.; Guo, Q.F.; Yan, Z.X.; Wang, M.L.; Pan, J.L. Investigating the Failure Mechanism of Jointed Rock Slopes Based on Discrete Element Method. *Adv. Civ. Eng.* **2020**, *2020*, 8820158. [CrossRef]
30. Zhu, C.; He, M.C.; Tao, Z.G.; Meng, Q.X.; Zhang, X.H. Recognition and prevention of rockfall vulnerable area in open-pit mines based on slope stability analysis. *Geomech. Eng.* **2021**, *26*, 441–452. [CrossRef]
31. Sun, L.; Liu, Q.S.; Abdelaziz, A.; Tang, X.H.; Grasselli, G. Simulating the entire progressive failure process of rock slopes using the combined finite-discrete element method. *Comput. Geotech.* **2022**, *141*, 104557. [CrossRef]

32. Sun, L.; Tang, X.H.; Abdelaziz, A.; Liu, Q.S.; Grasselli, G. Stability analysis of reservoir slopes under fluctuating water levels using the combined finite-discrete element method. *Acta Geotech.* **2023**, *18*, 5403–5426. [CrossRef]
33. Zhao, L.H.; Liu, X.N.; Mao, J.; Shao, L.Y.; Li, T.C. Three-dimensional distance potential discrete element method for the numerical simulation of landslides. *Landslides* **2020**, *17*, 361–377. [CrossRef]
34. Jia, J.; Pei, X.J.; Liu, G.; Cai, G.J.; Guo, X.P.; Hong, B. Failure Mechanism of Anti-Dip Layered Soft Rock Slope under Rainfall and Excavation Conditions. *Sustainability* **2023**, *15*, 9398. [CrossRef]
35. Li, X.S.; Li, Q.H.; Hou, G.Q.; Zhang, F.; Lu, J. Investigation on the disaster mechanism and dynamic evolution of a dump slope using experimental and numerical methods: Case study, Kunyang phosphate mine, China. *Geol. J.* **2024**, *59*, 1056–1071. [CrossRef]
36. *GB/T 50123-1999*; Standard for Soil Test Method. Chinese Standard: Beijing, China, 1999.
37. *GB/T 50266-2013*; Standard for Test Methods of Engineering Rock Mass. Chinese Standard: Beijing, China, 2013.
38. *GB 50330-2013*; Technical Code for Building Slope Engineering. Chinese Standard: Beijing, China, 2013.
39. *GB 50021-2001*; Code for Investigation of Geotechnical Engineering. Chinese Standard: Beijing, China, 2001.
40. Hua, J.X.; Zheng, J.G. Basic knowledge of geology and classification of rock and soil. In *Geological Engineering Handbook*, 5th ed.; China Architecture & Building Press: Beijing, China, 2018.
41. *GB 38509-2020*; Code for the Design of Landslide Stabilization. Chinese Standard: Beijing, China, 2020.

Disclaimer/Publisher's Note: The statements, opinions and data contained in all publications are solely those of the individual author(s) and contributor(s) and not of MDPI and/or the editor(s). MDPI and/or the editor(s) disclaim responsibility for any injury to people or property resulting from any ideas, methods, instructions or products referred to in the content.